Nuclear Instruments and Methods in Physics Research A 816 (2016) 62–69

Contents lists available at ScienceDirect

Nuclear Instruments and Methods in Physics Research A

journal homepage: www.elsevier.com/locate/nima

Analytical modeling for gamma radiation damage on silicon photodiodes

H. Jafari, S.A.H. Feghhi *

Radiation Application Department, Shahid Beheshti University, Tehran, Iran

ARTICLE INFO

Article history:
Received 23 August 2015
Received in revised form
20 January 2016
Accepted 26 January 2016
Available online 4 February 2016

Keywords:
Photodiode array
Geant4
Gamma dose
Analytical model

ABSTRACT

Radiation-induced damage in PIN silicon photodiode induces degradation of the photodiode parameters. In this work, by presenting an analytical model, the effect of gamma dose on the dark current in a PIN photodiode array was investigated. Geant4 was used to obtain the damage constant as a result of primary incident particle fluence and NIEL distribution calculations. Experimental measurements as well as numerical simulation of the semiconductor with ATLAS were carried out to verify and parameterize the analytical model calculations. A reasonable agreement has been found between analytical results and experimental data for BPX65 silicon photodiodes irradiated by a Co-60 gamma source at total doses up to 500 krad under different reverse voltages. Moreover, the results showed that the dark current of each photodiode array pixel has considerably increased by gamma dose irradiation.

1. Introduction

Real time imaging with ionizing radiations is commonly employed in many fields of research and industry [1–4]. Photodiode arrays are excellent candidates to replace position sensitive sensors in imaging systems [5–6]. The photodiode is a semiconductor device with a p–n junction or p–i–n structure (PIN), where light is absorbed in a depletion region and generates a photocurrent. A silicon p–i–n photodiode is similar to the ubiquitous p–n diode, except for a nearly intrinsic region between the two highly doped terminals. Such devices can be very compact, fast, highly linear, and exhibit a high quantum efficiency (i.e., generate nearly one electron per incident photon) and a high dynamic range; they can be operated in combination with suitable electronics and can be made in close packed arrays [7]. Since these devices are exposed to ionizing radiation in imaging processes, irradiation can cause defects in photodiodes. Therefore, the response of photodiodes from I-V characteristics can be investigated to determine their behavior and quality of them in radiation environments [8–10].

Radiation damage in semiconductor devices occurs when there is energy deposition in a sensitive volume of the device in the form of atomic displacement and/or electron ionization. The energy deposited as atomic displacement generates point defects (i.e. vacancies and interstitials) as well as cluster defects (i.e. high density defect regions) in the semiconductor lattice [11,12]. Moreover, due to the ionizing particle scattering, silicon atoms are displaced (Primary Knock on Atom or PKA) and travel within the lattice, inducing secondary defects by linking with the impurities present in silicon, and progressively losing their excess energy. At the end of the PKA recoil paths, dense defect agglomerations are formed, resulting in disordered regions usually referred to as clusters. These regions contain extremely high defect concentrations ($\sim 10^{19}$ cm^{-3}), which make possible direct charge exchange between trap levels [12].

The observed deterioration effects of radiation due to displacements of the lattice atoms in silicon devices depend on the fluence, particle type and energy. The non-ionizing energy loss transfer (NIEL) is introduced as the energy per unit path is lost by the incident particle for describing displacement processes. In case of Coulomb scattering of electrons on nuclei, the non-ionizing energy-loss can be calculated using the Mott differential cross-section which was expressed by Mott as two conditionally convergent infinite series in terms of Legendre expansions [13].

The direct charge exchanges result in enhanced generation rates, which are responsible for an increase in the leakage current [14]. Displacement damage causes degradation in silicon photodiode characteristics as verified in all types of silicon detectors [15]. The main parameter of the silicon photodiodes, which is expected to change after irradiation, is the effective dark current. As a mandatory step to assess the applicability of silicon PIN photodiode devices in a radiation environment, radiation tests must be performed to evaluate their response to radiation damage

* Corresponding author.
E-mail address: A_Feghhi@sbu.ac.ir (S.A.H. Feghhi).

http://dx.doi.org/10.1016/j.nima.2016.01.079
0168-9002/

[10]. Although in gamma irradiations, the densities of the primary defects are small compared to the densities that occur in neutron and protons irradiations at the end of a PKA cascade, produced electrons can generate considerable divacancies and vacancy complexes in silicon bulk. In contrast to the radiation damage introduced by high energy hadrons, an irradiation with Co-60 gammas can only create point defects. This provides an opportunity to investigate the isolated point defects without having to face the problems caused by the cluster effect [16,17].

The incorporation of radiation damage simulation capabilities into parametric analysis models is of great interest to the designers of integrated circuits that are used for radiation environments. This is mainly due to the fact that the use of commercial deep-submicron technologies has greatly increased for radiation applications [18–20]. These models represent the connection between descriptions of basic radiation damage effect mechanisms in devices and the practical art of IC design. As a consequence, precise modeling of the increase of trap density and carrier lifetime variations has a great practical value. The typical model involves the radiation damage mechanisms as well as the formation of deep traps at the silicon band gap due to the primary knock on silicon atoms [21].

In the present study, gamma radiation effects on silicon PIN photodiodes based on an analytical model has been investigated. The model is based on a numerical solution of partial differential equations with appropriate boundary conditions and parameters. Defects caused by Co-60 gamma radiation in silicon have been formulated in terms of the damage constant for the minority carriers' lifetime. Dark current has been analyzed in detail and results for commercial BPX65 photodiode devices have been obtained and compared with experimental data as well as the results of ATLAS semiconductor simulator.

2. Experimental setup

The radiation damage analysis was performed on a structure based on the silicon PIN photodiodes of BPX65. This photodiode is a family of semiconductor detectors featuring a Centronic's 1 mm^2 cross-sectional area, high speed, high sensitivity chip, which has already been successfully employed in a wide variety of applications [22]. The dark current of these photodiodes was measured employing a Keithley 485 Picoammeter. During the measurements, the photodiode was isolated in a dark box to avoid stray light which may bias the measurement. The reverse voltage was set by a Hameg HMP4030 programmable power supply.

The devices under test were irradiated by a Co-60 gamma source, with the energies of 1.33 and 1.17 MeV and dose rate of 271 rad/s (in Si). The photodiodes were exposed to an irradiation dose up to 500 krad (in Si). The components were irradiated in the air at a temperature of 21 °C. The results were obtained by averaging the parameters measured for five photodiodes at each dose level.

3. Analytic modeling

A simplified 1-D model has been used to describe the single photodiode behavior. However, surface effects and non-uniformities along the lateral direction are ignored. The most significant effect of gamma irradiation is the change in the device characteristics along the path of the collected signal charge. The free carriers (electron and hole) concentration and electrostatic potential through the device were extracted from the model. Therefore, the model includes three basic semiconductor equations (Poisson equation and continuity equation for electrons and holes) as represented by Eqs. ((1), (2) and (3)) respectively [23].

$$\frac{d^2\psi}{dx^2} = -\frac{q}{\varepsilon}[\Gamma + p - n - N_{eff}] \tag{1}$$

$$\frac{\partial n}{\partial t} = \frac{1}{q}\frac{dJ_n}{dx} - R \tag{2}$$

$$\frac{\partial p}{\partial t} = -\frac{1}{q}\frac{dJ_p}{dx} - R \tag{3}$$

where ψ is the electrostatic potential, ε is the dielectric permittivity of the material, q is the electron charge, n and p are the concentrations of electron and hole respectively, Γ is the net doping concentration, N_{eff} is the effective doping concentration, J_n and J_p represent the current densities of electrons and holes respectively, and R is the net recombination–generation rate. Current density expressions are also formulated on the basis of the drift-diffusion approach as represented by Eq. (4) for electrons [23].

$$J_n = q.D_n.\frac{dn}{dx} - q.n.\mu_n.\frac{d\psi}{dx} \tag{4}$$

where μ_n is the electron mobility; D_n is the electron diffusion coefficient. Similarly, the hole current density term is represented by hole continuity equation. This quantity can be used to obtain experimental observables such as dark current and photocurrent at given bias voltages.

The mechanisms of carrier generation and recombination in the semiconductors can be described by means of different models that show the physical behavior of the semiconductor. The thermal recombination–generation process via traps is represented by the Shockley–Read–Hall (SRH) Eq. (5) [24–26].

$$R_{SRH} = \frac{n.p - n_{int}^2}{\tau_n\left(p + n_{int}\exp\left(\frac{E_I - E_T}{kT}\right)\right) + \tau_p\left(n + n_{int}\exp\left(\frac{E_T - E_I}{kT}\right)\right)} \tag{5}$$

where n_{int} is the intrinsic carrier concentration, τ_n and τ_p are the minority carrier lifetimes of electrons and holes, respectively. Furthermore, E_T is the trap energy level, E_I is the intrinsic Fermi energy level, T is the lattice temperature and k is the Boltzmann constant.

The inclusion of damage to the silicon crystal was necessary to investigate the effect of gamma irradiation on the performance of the devices. This is implemented via the introduction of acceptor-like states situated deep in the forbidden gap of the semiconductor. These states are defined by the effective doping concentration (N_{eff}) as Eq. (6) [27].

$$N_{eff} = \sum N_T f(E_T) \tag{6}$$

where, N_T represents the density of trap levels introduced during irradiation and $f(E_T)$ is the electron occupation function where fraction of filled trap levels at energy E_T is expressed by Eq. (7) [24].

$$f(E_T) = \frac{\tau_p.n + \tau_n.n_{int}\exp\left(\frac{E_I - E_T}{kT}\right)}{\tau_p\left(n + n_{int}\exp\left(\frac{E_T - E_I}{kT}\right)\right) + \tau_n\left(p + n_{int}\exp\left(\frac{E_I - E_T}{kT}\right)\right)} \tag{7}$$

Subsequently, the minority carrier lifetimes of electrons and holes are represented by Eq. (8).

$$\tau_{n,p} = \frac{1}{C_{n,p}.N_T} \tag{8}$$

where $C_{n,p}$ are the capture rates for either electrons and holes, defined as $C_{n,p} = \sigma_{n,p}.v_{n,p}$, in which $\sigma_{n,p}$ is the capture cross-section (see Table 2 below) for electrons (holes) and $v_{n,p}$ as the carrier thermal velocities.

The increase in dark current during gamma irradiation is due to the introduction of recombination centers with energy levels deep in the forbidden gap of the semiconductor. This leads to an

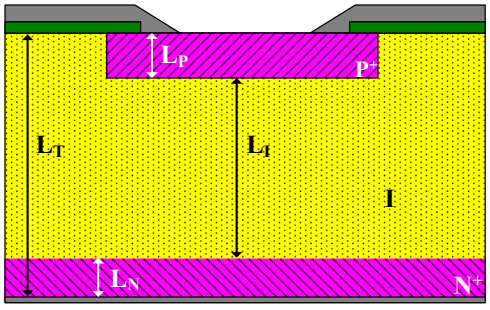

Fig. 1. The scheme of simulated PIN photodiode.

Table 1
The specification of implants for simulated BPX65 photodiode structure.

Implant	Peak level [cm^{-3}]	Depth [μm]
P+	1×10^{18}	2.25
N+	1×10^{18}	2.25
I	1.5×10^{14}	27.75

Table 2
Main parameters used in ^{60}Co-gamma-irradiated samples.

Parameter	Values
Electrons capture cross-section (σ_n)	1.48×10^{-14} cm^2
Holes capture cross-section (σ_p)	1.48×10^{-14} cm^2

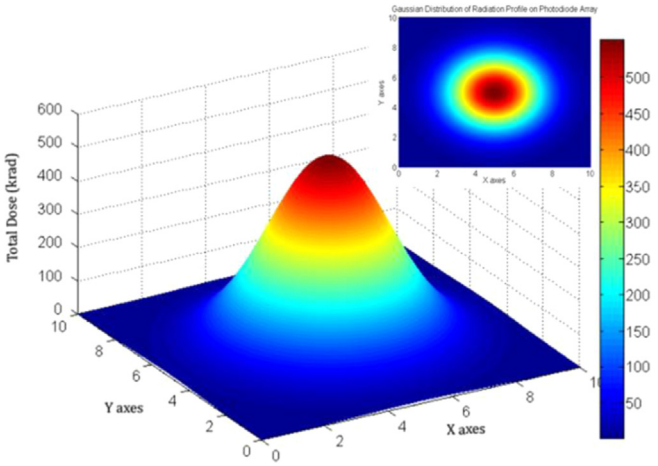

Fig. 2. Gaussian distribution of total ionizing dose on simulated photodiode array.

increase in the thermal generation of charge carriers. This process is described in the simulation via the modification of the minority carrier lifetime which controls the SRH thermal generation-recombination term in the continuity equations. The variation in minority carrier lifetime with incident particle fluence, Φ, in silicon under equilibrium conditions, was described in terms of the lifetime damage-constant, K_τ as expressed by Eq. (9) [11].

$$\frac{1}{\tau_r}=\frac{1}{\tau_{r_0}}+K_\tau\Phi \tag{9}$$

where τ_{ro} and τ_r are the carrier lifetimes before and after irradiation respectively. The lifetime damage-constant characterizes the detailed phenomenological information relating to the physical interactions between the incident particles and the semiconductor material. Many experimental investigations have shown that to first order one might assume a linear proportionality, independent of the particle, between the lifetime damage-constant and the particle NIEL [28]. This is the essence of the use of the NIEL parameter since it allows to measure K_τ only for one particle (at one specified energy) from which the K_τ values for all particles (and energies) are easily estimated. Therefore, we use Eq. (10) to find the lifetime damage-constant for Co-60 ($K_{\tau\gamma}$).

$$\frac{K_{\tau\gamma}}{K_{\tau n}}=\frac{\mathrm{NIEL}_\gamma}{\mathrm{NIEL}_n} \tag{10}$$

Here, we considered $K_{\tau n}=10^{-7}$ cm^2/s for 1 MeV neutrons with the NIEL_n value of 2.04×10^{-3} MeV cm^2/g in silicon which were obtained by Akkerman et al. [29]. Therefore, we needed to calculate the NIEL_γ for predicting the carrier lifetimes degradation of silicon photodiode device due to the Co-60 irradiation. For the displacement damage caused by nuclear particle and gamma ray induced secondaries, it is difficult to obtain the NIEL directly from the experiment, because of the short range of the recoils. The main approach is thus to use theoretical calculations. Such calculations have been performed by several authors in the frame of various theoretical models of nuclear interaction of these particles with the device-material nuclei [30].

Since the evaluation of the NIEL should involve proper treatment of each interaction physics, a charged particle Monte Carlo code with complete cross-section library can be used. Geant4 is a Monte Carlo code for transport radiation through the matters. This code has been developed in C++ language and has been applied frequently in space radiation study, microdosimetry, medical application etc. It includes different models to calculate particle interaction in a wide range of energy [31,32]. Therefore, Geant4 has been used to calculate the electron fluence and NIEL produced by gamma irradiation in sensitive volume of silicon PIN photodiode.

On the other hand, the increase in dark current (I_{DC}) is related to the minority carrier lifetime of the photodiode as Eq. (11) if the generation-recombination is dominated by midband levels caused by defects [33]:

$$I_{DC}=\frac{qwAn_{int}}{2\tau} \tag{11}$$

where, w is depletion depth of photodiode and A is the active area. Therefore, the variation in the dark current induced by incident particle fluence, Φ, is achieved by substituting the carrier lifetime in the Eq. (11) with the Eq. (9). The difference between the dark current before and after irradiation is represented by ΔI_{DC} as Eq. (12).

$$\Delta I_{DC}=K_R\Phi \tag{12}$$

The device parameters can be absorbed into the constant by defining a new damage-constant (K_R) which is given by Eq. (13).

$$K_R=qwAn_{int}K_\tau \tag{13}$$

In general, this damage-constant in semiconductors depend on the parameters such as type and energy of the incident particle, kind of material, resistivity, types and concentration of impurities, injection level, temperature and elapsed time after irradiation [10,34]. The damage-constant (K_R), in this work, has been determined experimentally by performing photodiode dark current measurements for a particular set of device operating conditions after incremental gamma exposures at a given fluence of produced electron.

A finite-difference approach has been used to solve Eqs. (1), (2) and (3) in one dimension with the appropriate boundary conditions. Then, the potential and free carrier densities have been calculated at each node, which subdivide the solution domain, by means of the Scharfetter-Gummel method (an iterative numeric method) [35]. Knowing of these quantities allows calculating the dark current with the purpose of evaluating the radiation-induced

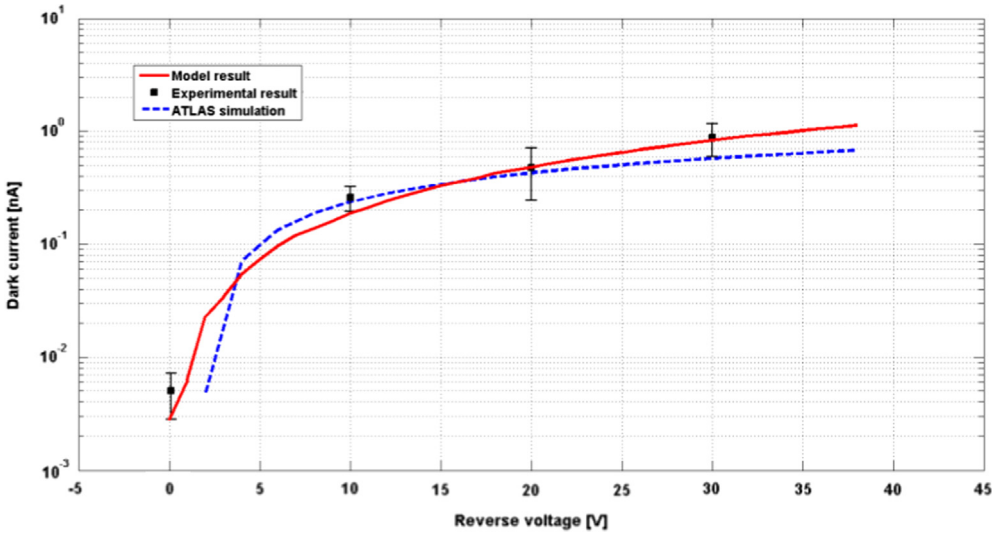

Fig. 3. Dark current as function of reverse voltage for BPX65 PIN silicon photodiode.

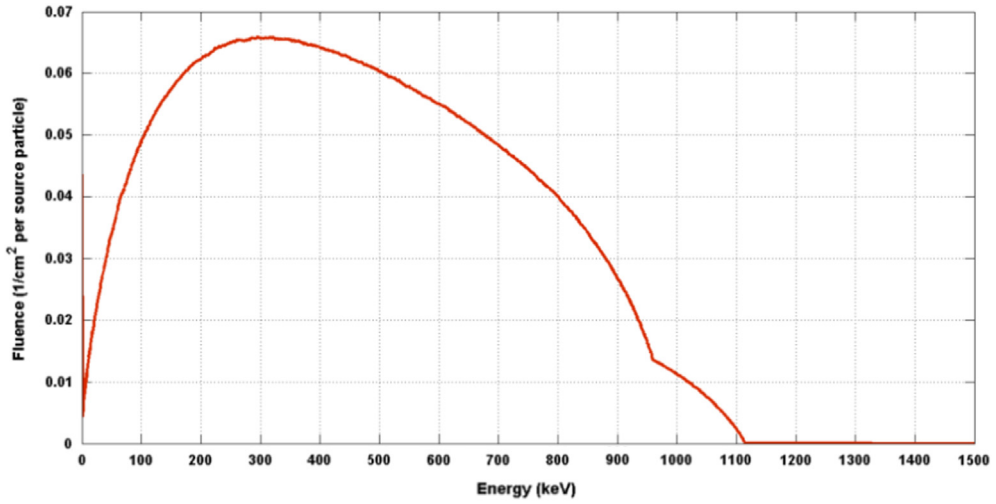

Fig. 4. The energy distribution of primary electrons fluence from Co-60 gamma irradiation per source particle in simulated structure of BPX65 silicon photodiode.

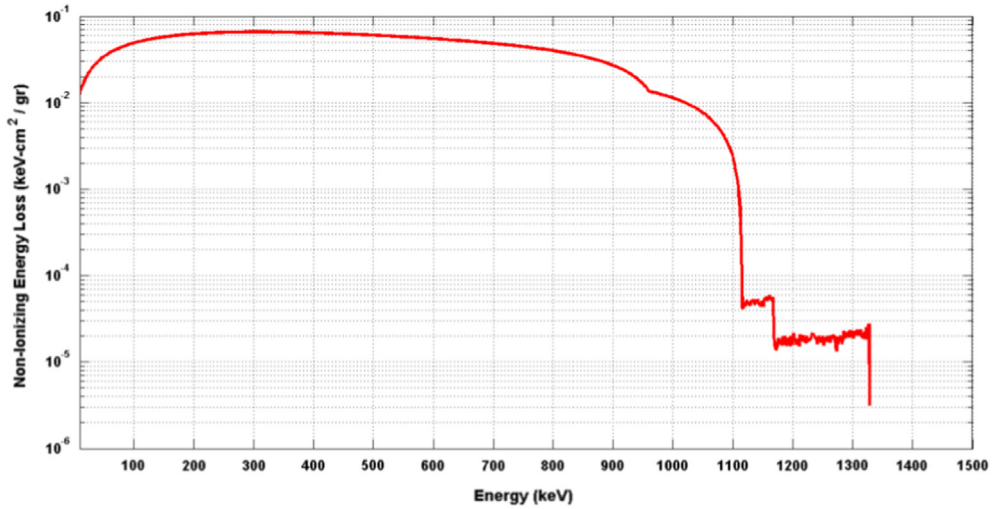

Fig. 5. The NIEL distribution of primary electron from Co-60 gamma irradiation as function of electron energy in simulated structure of BPX65 silicon photodiode.

traps on the analyzed devices. The calculation process was repeated until the relative error at each grid-point fell below a predetermined level. Generally a value of 1×10^{-10} was used as this was the limit that could be achieved for initial solutions.

In addition, radiation-induced degradation can be calculated numerically using semiconductor device simulators. ATLAS is one of the physically-based commonly used device simulators, which can predict the electrical characteristics associated with specified physical structures and bias conditions [36]. Steady state, transient, AC-small signal and optical device simulation can be performed with this simulator.

Due to the lack of a precise description of the real PIN photodiode (BPX65), we used approximated values for our simulations. Fig. 1 shows the schematic diagram of simulated PIN photodiode. L_P, L_I and L_N are the thicknesses of P+, intrinsic and N+ regions, respectively. Actually, the intrinsic layer is not a pure silicon region but a slightly n-type doped one [37]. The parameters of the various implants for BPX65 photodiode are detailed in Table 1.

It has been assumed that gamma penetrates into the device through all directions. As described, reasonable dimensions of the layer and doping profiles (with Gaussian distribution) have been adopted for device simulation purposes, with L_T=30 μm, L_I=27.75 μm, L_P=L_N=2.25 μm and active area of 1 mm^2. The deep level traps were considered as a uniform distribution.

The most likely candidate for the deep acceptor level related damage after Co-60 irradiation detectable with the DLTS method is the VO_i complex which is situated 0.17 eV below the conduction band (E_C–0.17 eV) [38]. Most relevant simulation parameters are summarized in Table 2.

A 2-D PIN silicon photodiode array with 10×10 elements was simulated to investigate the variation of dark current due to irradiation on the pixels. The irradiation was considered by total ionizing dose with Gaussian distribution on the photodiodes. Fig. 2 shows the desired dose distribution which includes mean value of 550 krad and standard deviation of 1.7.

Table 3
The trap densities of silicon PIN photodiodes for several total doses of Co-60 irradiation.

Total dose (krad)	Trap density [N_T] (cm^{-3})		
	Experimental estimate	Model estimate	Relative difference (%)
10	5.50×10^{9}	4.95×10^{9}	10.0
50	2.75×10^{10}	2.99×10^{10}	8.72
100	5.50×10^{10}	5.45×10^{10}	0.90
200	1.10×10^{11}	1.34×10^{11}	21.81
500	2.75×10^{11}	2.61×10^{11}	5.09

4. Results

The dark current versus reverse bias characteristic for BPX65 PIN silicon photodiode before irradiation is shown in Fig. 3. The results associated with the analytical model, experimental data and ATLAS simulations have been compared.

As depicted in Fig. 3, the dark current of the desired photodiode increases with reverse voltage. The dark current was 0.882 nA

Table 4
The damage-constants of silicon PIN photodiodes at different reverse voltages for Co-60 gamma source in several total doses.

Total dose (krad)	Damage constant [K_R] (pA cm^2)							
	Experimental estimate				Model estimate			
	Reverse voltage=1 V	Reverse voltage=10 V	Reverse voltage=20 V	Reverse voltage=30 V	Reverse voltage=1 V	Reverse voltage=10 V	Reverse voltage=20 V	Reverse voltage=30 V
10	1.01×10^{-17}	9.83×10^{-17}	1.53×10^{-16}	9.86×10^{-16}	8.99×10^{-18}	1.35×10^{-16}	2.09×10^{-16}	1.22×10^{-15}
50	4.16×10^{-17}	1.08×10^{-16}	5.28×10^{-16}	9.92×10^{-16}	2.31×10^{-17}	1.94×10^{-16}	6.45×10^{-16}	1.38×10^{-15}
100	6.67×10^{-17}	1.33×10^{-16}	7.33×10^{-16}	1.53×10^{-15}	5.48×10^{-17}	2.03×10^{-16}	7.67×10^{-16}	1.95×10^{-15}
200	9.97×10^{-17}	4.98×10^{-16}	8.31×10^{-16}	1.03×10^{-15}	5.90×10^{-17}	5.60×10^{-16}	9.14×10^{-16}	2.17×10^{-15}
500	5.31×10^{-17}	5.57×10^{-16}	9.28×10^{-16}	1.30×10^{-15}	6.74×10^{-17}	5.97×10^{-16}	9.98×10^{-16}	2.40×10^{-15}

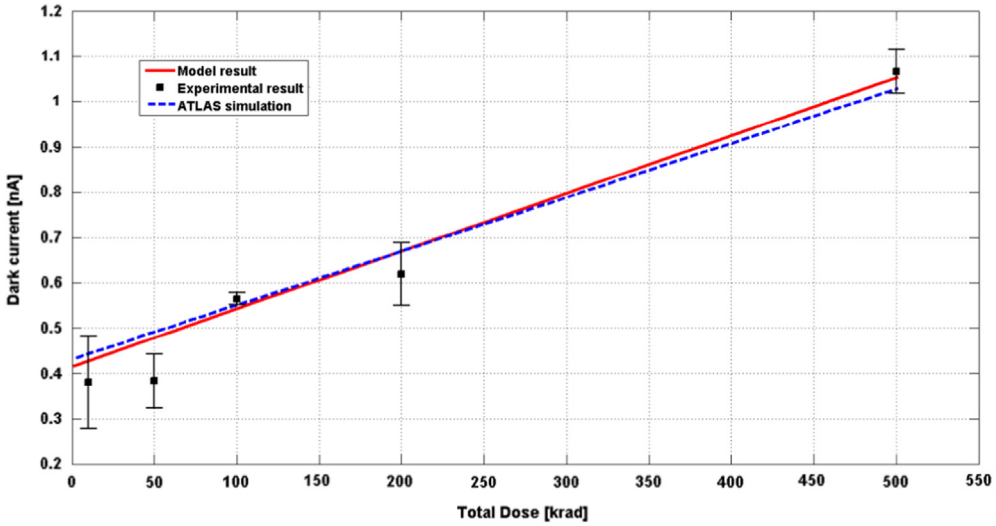

Fig. 6. The dark current of BPX65 photodiode as function of total dose under reverse voltage of 20 V.

under reverse voltage of 30 V before irradiation. There is an acceptable agreement between model results, ATLAS simulations and experimental data. The ATLAS simulation results reveal approximately 15% relative difference in comparison with experimental data while the model displays approximately 6% difference.

The described silicon photodiodes were irradiated with total dose levels up to 500 krad by a Co-60 gamma source. As illustrated, Compton electrons generated by incident photons, are responsible for displacement of the lattice atoms in this structure. The distribution of primary electron fluence was calculated using Geant4 in silicon structure of desired photodiodes. The energy distribution of primary electrons fluence from a Co-60 gamma irradiation per source particle in simulated photodiode structure is shown in Fig. 4. Moreover, Fig. 5 shows the NIEL distribution of produced electron in silicon photodiode.

Therefore according to Eq. (10), the calculation of $NIEL_\gamma$ using the values in Fig. 5 gives $K_\tau = 5 \times 10^{-12}$ cm^2/s. In addition, the density of trap levels, N_T, is related to the irradiation dose by its introduction rate K_I as given in Eq. (14) [27].

$$N_T = K_I D \tag{14}$$

Where D is total gamma dose. The value of the introduction rate was determined for the VO_i trap level after Co-60 irradiation of silicon photodiode to be $K_I = 5.5 \times 10^5$ Rad^{-1} cm^{-3} as reported by Moll et al. [16]. It is an experimental estimate which compared with our model estimate calculation for several total doses of Co-60 gamma irradiation as presented in Table 3.

In addition, the values of damage-constant K_R, which were obtained by Geant4 calculation of NIEL (Eq. 13) and measured variation in dark current before and after irradiation (Eq. 12) for different reverse voltages are summarized in Table 4. It can be clearly seen that the dark current of silicon PIN is greatly dependent on the photodiode reverse voltage.

As illustrated, the minority carrier lifetime of the device decreases with increasing primary electron fluence in a silicon photodiode structure from a Co-60 gamma source. Fig. 6 shows the relation between the dark current of BPX65 photodiode and the total dose under reverse voltage of 20 V which was obtained from the analytical model together with the experimental data and ATLAS simulation results. Since the photodiodes are not identical, the measured dark current was obtained by averaging over five different photodiodes for each dose level. Therefore, according to the measured dark currents, one-sigma standard deviations were obtained between 0.01 nA and 0.1 nA which are respectively pertaining to 100 krad and 10 krad irradiation dose.

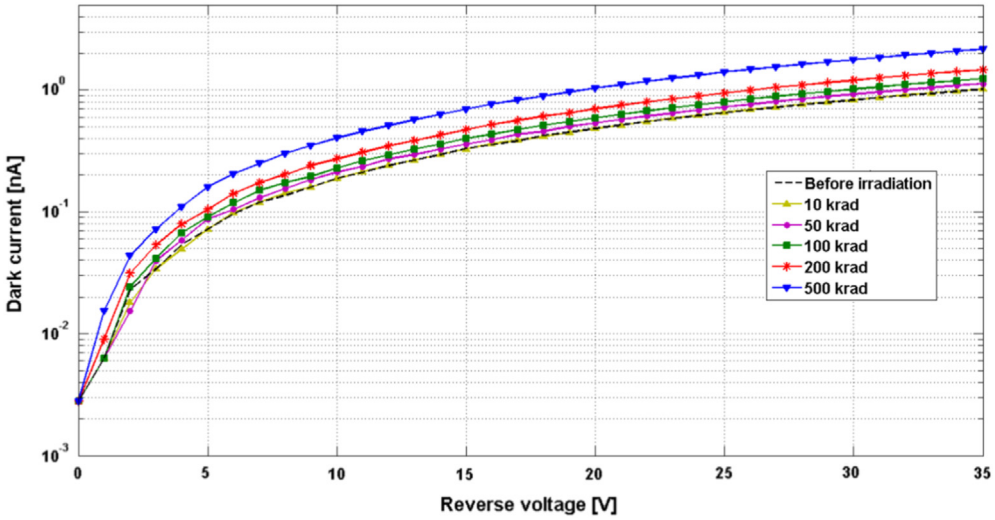

Fig. 7. The dark current of BPX65 photodiode as function of reverse voltage at several dose levels.

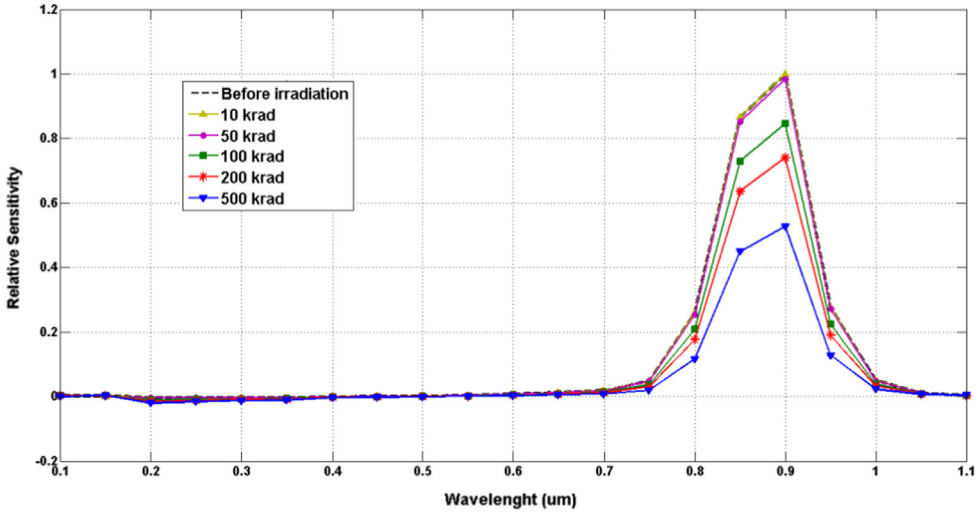

Fig. 8. Relative spectral sensitivity of BPX65 photodiode at several dose levels.

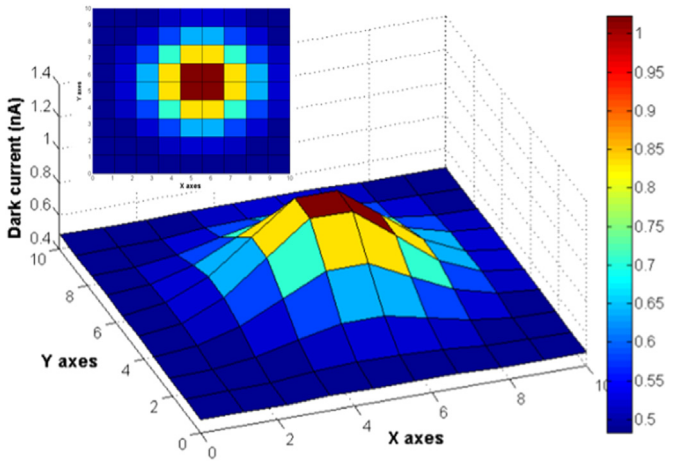

Fig. 9. The Dark current profile concern with simulated irradiation on photodiode array.

It can be noticed that the dark current increases linearly with total dose. The dark current of the BPX65 photodiode is calculated to be 1.013 nA at total dose of 500 krad which was about 2 times greater than its value before irradiation. The maximum relative difference between experimental and model calculation results is 6.2% which is 1% between ATLAS results and model calculation. The dark current results from analytical modeling for five dose levels irradiation as function of reverse voltage are shown in Fig. 7.

It can be seen that the difference of photodiode dark current before and after irradiation increases with the increase of reverse voltage. Thus, the differences between dark currents before and after 500 krad total dose irradiation were 9.01×10^{-3}, 4.10×10^{-1} and 9.84×10^{-1} nA at reverse voltages of 1 V, 15 V and 30 V respectively. The normalized photocurrent spectrum of PIN photodiode is shown in Fig. 8 for various total doses.

The maximum sensitivity of simulated structure of desired photodiode was obtained at wavelength about 900 nm. The photocurrent is attenuated with an increasing total dose. Hence, the photocurrent for a total dose of 500 krad becomes 2 times less than before irradiation.

The dark current results, which are obtained from a single silicon photodiode using developed analytical model, have been employed to predict the behavior of a photodiode array at Co-60 gamma irradiation. Therefore, an array with 10×10 pixels was simulated. The variation of dark current due to the considered irradiation on the array under reverse voltage of 20 V was calculated as shown in Fig. 9. It can be seen that the related dark current of each pixel has been modeled proportionally to the gamma irradiation dose on photodiode array. Therefore, the pixel corresponding to maximum irradiation (550 krad) exhibits a dark current of 1.02 nA.

5. Conclusion

Radiation effect modeling on a silicon photodiode array requires analyzing the basic mechanism resulting in the formation of deep traps at silicon band gap due to the primary knock on silicon atoms of each single photodiode. In this study an analytical model was utilized based on general equations describing the generation, transport and trapping of mobile species to investigate radiation-induced degradation parameters of BPX65 as a PIN silicon photodiode. The verification of results was carried out by comparing them with experimental data as well as the results of a numerical semiconductor simulation code (ATLAS) for the irradiation by a Co-60 gamma source in several total doses under different reverse voltages. In addition, Geant4 calculations were performed to obtain the damage constant from the primary electron fluence and the NIEL distribution of produced electrons in a silicon photodiode which was about 5×10^{-12} cm^2/s.

The dark current of the simulated single photodiode structure increased from 0.437 nA at the time before irradiation to 1.013 nA at total dose of 500 krad under reverse voltage of 20 V. Moreover, the photocurrent was attenuated by a factor of 2 after irradiation at total dose of 500 krad. The calculation results showed good agreement with experimental data and ATLAS simulations of the irradiated BPX65 silicon photodiode by a Co-60 gamma source (with the dose rate of 0.2 rad/s in Si) in several total doses and different reverse voltages. Finally, the model has been applied to the estimation of dark current and radiation effects of a (10×10 pixels) photodiode array. Generally, because of the predictive nature of these devices, a proper parameterization of the model allows extrapolating the calculations to higher doses for high level dose applications.

Acknowledgment

We would like to express our appreciation to Mr. Saeed Boorboor for his help in performing the experimental data analysis and his valuable suggestions while planning this research work.

References

[1] D.A. Garrett, D.A. Bracher, Real-time radiologic imaging: medical and industrial applications, ASTM STP 716, American Society for Testing and Materials, 1980.
[2] Z.H. Cho, J.P. Jones, M. Singh., Foundations of Medical Imaging, Wiley, New York, 1993.
[3] H.S. Cho, et al., Nuclear Instruments and Methods in Physics Research Section A 652 (1) (2011) 650.
[4] A. Rappoldi, Nuclear Instruments and Methods in Physics Research Section A 610 (1) (2009) 291.
[5] R.A. Metzler, A.O. Goushcha, C. Hicks, and E. Bartley, Ultra-thin, two dimensional, multi-element Si pin photodiode array for multipurpose applications. in: Semiconductor Photodetectors, Proceedings of SPIE 5353, SPIE, Bellingham, WA, 2004, pp. 117–125.
[6] A. Jucha, D. Bonin, E. Dartyge, A.M. Flank, A. Fontaine, D. Raoux, Nuclear Instruments and Methods in Physics Research Section A 226 (1) (1984) 40.
[7] D.A. Bell, Fundamentals of Electronic Devices and Circuits, Oxford University Press, 2009.
[8] K. Teraoka, et al., Nuclear Instruments and Methods in Physics Research Section A 324 (1–2) (1993) 276.
[9] J. Wiczer, C. Barnes, IEEE Transaction on Nuclear Science 29 (1982) 1539.
[10] M. McPherson, B.K. Jones, T. Sloan, Semiconductor Science and Technology 12 (1997) 1187.
[11] G.C. Messenger, M.S. Ash, The Effects of Radiation on Electronic Systems, van Nostrand Reinhold, New York, 1986.
[12] J.R. Srour, C.J. Marshall, P.W. Marshall, IEEE Transaction on Nuclear Science 50 (2003) 653.
[13] N.F. Mott, Proceedings of the Royal Society of London. Series A, 124 (794) (1929) 425.
[14] S.J. Watts, et al., IEEE Transaction on Nuclear Science 43 (1996) 2587.
[15] C. Leroy, P.G. Rancoita, Reports on Progress in Physics 70 (2007) 403.
[16] M. Moll, et al., Nuclear Instruments and Methods in Physics Research Section A 388 (3) (1997) 335.
[17] M. Gökçen, A. Tataroglu, S. Altindal, M.M. Bülbül, Radiation Physics and Chemistry 77 (1) (2008) 74.
[18] S.M. Eladl, Microelectronics Journal 40 (2009) 193.
[19] H. Jafari, S.A.H. Feghhi, Nuclear Instruments and Methods in Physics Research A 777 (2015) 28.
[20] H.J. Barnaby, M.L. McLain, I.S. Esqueda, X.J. Chen, IEEE Transactions on Circuits and Systems I: Regular Papers 56 (2009) 1870.
[21] M.A. Cappelletti, U. Urcola, E.L. Peltzer y Blanca, "Radiation-Damaged Simulation PIN Photodiodes", Semiconductor Science and Technology 21 (2006) 346.
[22] BPX65 Silicon p-i-n Photodiode Datasheet, Available: http://www.centronic.co.uk
[23] S.M. Sze, K.K. Ng, Physics of Semiconductor Devices, third ed., Wiley, New York, 2006.
[24] W. Shockley, W.T. Read, Physical Review 87 (5) (1952) 835.
[25] R.N. Hall, Physical Review 87 (2) (1952) 387.

[26] M.A. Lampert, Physical Review 103 (1648) (1956).
[27] J. Matheson, M.S. Robbins, S.J. Watts, Nuclear Instruments and Methods A 377 (1996) 224.
[28] C.J. Marshall, P.W. Marshall, IEEE NSREC Short Course 12 (1999) IV50.
[29] A. Akkerman, et al., Radiation Physics and Chemistry 62 (2001) 301.
[30] S.R. Messenger, et al., IEEE Transactions on Nuclear Science NS46 (1999) 1595.
[31] S. Agostinelliae, et al., Nuclear Instruments and Methods in Physics Research A 506 (2003) 250.
[32] S. Boorboor, S.A.H. Feghhi, H. Jafari, Radiation Measurements 78 (2015) 42.
[33] D.K. Schroder, IEEE Transactions on Electron Devices ED29 (1982) 1336.
[34] J.R. Srour, D.H. Lo, IEEE Transactions on Nuclear Science NS47 (2000) 2451.
[35] H. Gummel, IEEE Transactions on Electron Devices (1964) 455–465.
[36] ATLAS User's Manual, In: Silvaco, Ed., ed. Santa Clara, United States, 2012.
[37] L. Dehimi, N. Sengouga, B.K. Jones, Nuclear Instruments and Methods in Physics Research Section A 519 (3) (2004) 532.
[38] J.W. Corbett, G.D. Watkins, R.M. Chrenko, R.S. McDonald, Physical Review 121 (4) (1961) 1015.